

Gate-Controlled Spin Injection at LaAlO₃/SrTiO₃ Interfaces

N. Reyren,¹ M. Bibes,¹ E. Lesne,¹ J.-M. George,¹ C. Deranlot,¹ S. Collin,¹ A. Barthélémy,¹ and H. Jaffrès^{1,*}

¹Unité Mixte de Physique CNRS-Thales, 1 Av. A. Fresnel, 91767 Palaiseau, France and Université Paris-Sud, 91405 Orsay, France
(Received 25 November 2011; published 30 April 2012)

We report results of electrical spin injection at the high-mobility quasi-two-dimensional electron system (2-DES) that forms at the LaAlO₃/SrTiO₃ interface. In a nonlocal, three-terminal measurement geometry, we analyze the voltage variation associated with the precession of the injected spin accumulation driven by perpendicular or transverse magnetic fields (Hanle and inverted Hanle effect). The influence of bias and back-gate voltages reveals that the spin accumulation signal is amplified by resonant tunneling through localized states in the LaAlO₃ strongly coupled to the 2-DES by tunneling transfer.

DOI: 10.1103/PhysRevLett.108.186802

PACS numbers: 73.20.-r, 72.25.Hg, 73.40.-c, 85.75.-d

The LaAlO₃/SrTiO₃ (LAO/STO) system is the subject of intense research [1–3] due notably to its two-dimensional highly conductive character. Among other remarkable properties, LAO/STO shows superconductivity [4], giant gate tunability in the normal [5] or superconducting state [6,7] and a large modulation of Rashba spin-orbit interactions [8,9] imposed by the strong electric field at the interface [10]. Besides their potential for electronics [11,12], the high electronic mobility and two-dimensional character make this 2-DES an interesting platform to explore lateral spin transport in oxide heterostructures. Spintronics with oxide systems could take advantage of the variety of functional materials existing in this family, including ferroelectrics or multiferroics. The integration of such materials is readily achievable because epitaxial growth of oxide heterostructures is well controlled today, paving the way towards novel multifunctional spintronics architectures.

In a spin injection device, polarized electrons are traditionally injected from a ferromagnetic (FM) electrode into a channel by passing a current from the FM into the channel (here the 2-DES) through a tunnel contact. The induced imbalance of spin population at the channel side, called spin accumulation, creates a finite additional voltage at the FM/2-DES contact. The contribution of this spin-accumulation-generated voltage to the total voltage measured between the top Co electrode and an Ohmic reference contact (far from the injection region) may be revealed in a three-point measurement scheme [Fig. 1(a)] by measuring the electrical Hanle effect. Conventionally, the Hanle effect is observed by applying an external magnetic field perpendicular to the FM injector's magnetization, in order to drive an incoherent precession of the injected electronic spins, which suppresses spin accumulation. This leads to a *negative* magnetoresistance, that is a drop of resistance vs magnetic field, with a typical Lorentzian shape, at least for localized electrons.

Inversely, the possible existence of a local *random* magnetic field within the 2-DES or at the proximity of FM/2-DES contact, and responsible for a partial spin depolarization at zero external field, can be probed by

applying the magnetic field parallel to the FM magnetization [Fig. 1(a)] [13]. As the applied magnetic field increases, the spin depolarization due to the random field is progressively suppressed, which restores the maximum spin accumulation. This leads to *positive* magnetoresistance or *inverted* Hanle effect with a width characteristic of the amplitude of the random field.

In this Letter, we report an important step towards prospective oxide-based spin injection devices. Namely, we demonstrate efficient electrical spin injection at the LAO/STO oxide interface via Hanle measurements, in the vein of what was recently demonstrated in devices based on conventional semiconductors [13–21]. Here, we also get further insights in the process of spin injection using a back-gate-voltage that modulates the density of states at the interface with the 2-DES. By means of combined Hanle and inverted Hanle measurements [Fig. 1(a)], we demonstrate the creation of a spin accumulation close to the LAO/STO interface. The total Hanle signal, of very large amplitude compared to our theoretical estimate, is

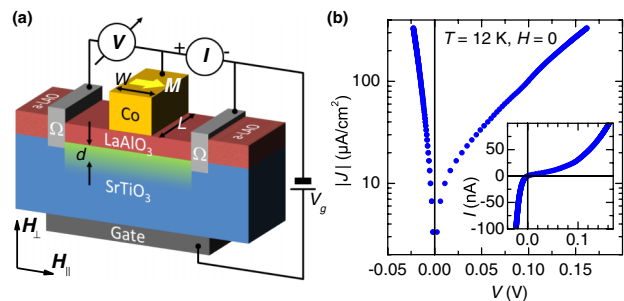


FIG. 1 (color online). (a) Sketch of the devices for 3-T Hanle measurements with the magnetic field applied perpendicular or parallel to the sample plane. A gate voltage V_g can be applied between the back of the STO crystal and the LAO/STO 2-DES. “a-LAO” stands for amorphous LaAlO₃, “Ω” for Ohmic contact, and the 2-DES is shown in green. M is the in-plane Co electrode magnetization. (b) Typical I vs. V characteristics of a Co/LaAlO₃/SrTiO₃ ($L = 100 \mu\text{m}$, $W = 300 \mu\text{m}$) sized junction measured at 12 K.

interpreted as the result of a resonant spin injection process into discrete electronic states strongly coupled to the 2-DES by tunneling transfer.

Samples were prepared by pulsed laser deposition (PLD) by first growing a pattern of amorphous LAO film [22] at room temperature on a (001)-oriented TiO₂-terminated STO substrate and then growing a four to five unit cell thick LAO film at high temperature [1,5,23]. An *in situ* post-annealing is realized at more than 500 °C in ~0.5 bar of O₂ for 30 to 60 minutes in order to reduce as much as possible the concentration of oxygen vacancies [23,24]. After deposition of the LAO film, a 15 nm thick Co ferromagnetic top electrode was deposited at room temperature by sputtering and then capped *in situ* with gold. The LAO film being a band insulator with a 5.6 eV band gap, it plays the role of the tunnel barrier required for an efficient spin injection [25] from the Co to the 2-DES in STO. The resulting device is illustrated in the Fig. 1(a) after the lithographic process. From an electrical point of view, *I-V* data acquired at low temperature [Fig. 1(b)] display a clear tunneling behavior characterized by a strong asymmetry between positive and negative bias (positive bias means that electrons are injected from the 2-DES into Co). Such an asymmetry is likely imposed by the difference of materials work function (as also found in Ref. [26] for Pt/LAO/STO and Au/LAO/STO) and probably reflects the strong trapezoidal shape of the LAO barrier in these junctions.

We now focus on electrical spin injection measurements. We collected standard 3-terminal magnetoresistance (MR) data on Co/LAO/STO junctions with a typical area $A = LW = 100 \times 300 \mu\text{m}^2$ [see Fig. 1(a)] by applying an out-of-plane magnetic field H_{\perp} normal to the Co in-plane magnetization [14,15]. Results at 2 K are presented in Fig. 2(b). After subtraction of a parabolic background, a negative MR with a quasi-Lorentzian shape is observed, corresponding to the normal Hanle effect. The amplitude of this Hanle signal is $\Delta R_{H\perp}A = 60 \text{ M}\Omega \cdot \mu\text{m}^2$, which, using a base junction resistance area product (RA) of $80 \text{ G}\Omega \cdot \mu\text{m}^2$, corresponds to an $MR = \Delta R_{H\perp}A/RA$ of 0.07%. The increase of resistance above about 0.3 T is at least partly related to the rotation of the Co electrode magnetization M out-of-plane (that would be complete for $\mu_0 H_{\perp} > 1.8 \text{ T}$).

As visible on Fig. 2(a) the junction resistance strongly increases with decreasing temperature, signaling thermally activated tunneling conduction through electronic localized states (ELS). Figure 2(c) displays Hanle effect curves at temperatures between 2 and 150 K. The Hanle signal remains about constant between 2 and 40 K where the RA vs temperature dependence [Fig. 2(a)] reaches a plateau. In contrast, no Hanle signal is obtained at higher temperature or at reversed bias. This is likely due to multistep (more than two) tunneling processes, since electrons that are thermally excited can access more states in the barrier.

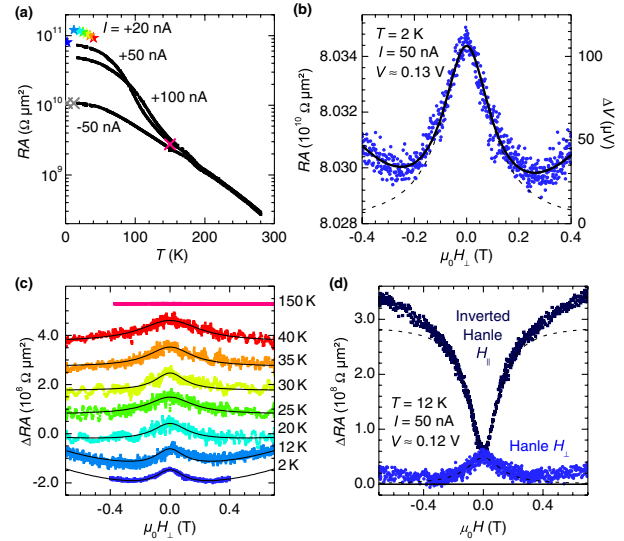


FIG. 2 (color online). (a) Temperature T dependence of the junction RA product measured at $I = +100$, $+50$ and -50 nA in black; the colored symbols correspond to the RA value for $I = +20$ nA as shown in (c) We used \star to indicate the observation of an Hanle effect and \times if not. (b) RA product and voltage change as a function of the perpendicular external magnetic field H_{\perp} (Hanle measurement). Lines correspond to Lorentzian fits of the data with (solid line) or without (dashed line) a parabolic background. (c) Hanle data acquired at different temperatures for $I = +20$ nA except for 2 K and 150 K for which $I = +50$ nA. The curves are vertically offset for the sake of clarity. (d) MR with the magnetic field perpendicular or parallel to the sample plane at 12 K for the same injected current of $I = +50$ nA. The dashed lines correspond to Lorentzian fits without the parabolic background.

We infer that the relevant ELS energy levels involved in the transport are located close to the Fermi energy of the 2-DES as in the sketch of Fig. 3. Owing to the band structure articulation at the LAO/STO interface [27] and to the calculated position of the electronic level of intrinsic defects in LAO [28,29], such ELS are likely played by remaining oxygen vacancies or cation intermixing [30,31].

The observed Hanle data reflect a correlated drop (as H is increased) of the spin splitting $\Delta\mu = \mu_{\uparrow} - \mu_{\downarrow}$ and voltage ΔV according to $\Delta V = |\gamma\Delta\mu/(2e)|$ [32], with $\mu_{\uparrow,\downarrow}$ the respective electrochemical potential for majority \uparrow and minority \downarrow spin channel, and γ the tunneling spin polarization at Co/LAO interface [33]. A primary analysis would lead to a splitting of the chemical potential $\Delta\mu(H)$ of the simplest form $\Delta\mu(0)/[1 + (\omega_L\tau_{sf})^2]$, where ω_L stands for the Larmor frequency, and τ_{sf} the spin-relaxation time extracted from the width of the Lorentzian [16]; this would give $\tau_{sf} \approx 50 \text{ ps}$ with $g_e = 2$. However, the width of the Lorentzian may be extrinsically enlarged in the presence of alternative mechanisms of spin depolarization near the interface, such as random magnetic fields due to stray fields, hyperfine interactions, etc. [13].

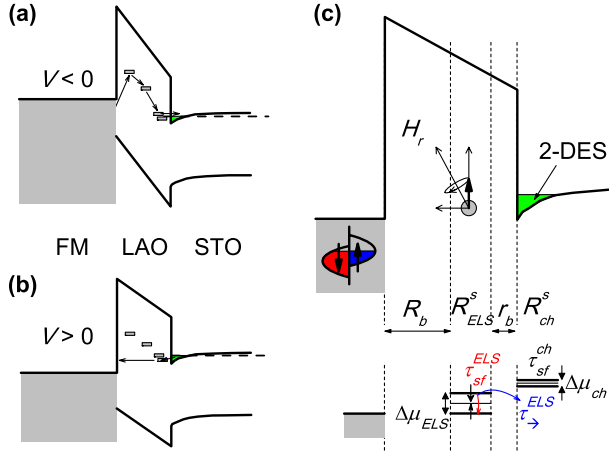


FIG. 3 (color online). Sketch of the band structure and electronic localized states in the barrier for (a) negative and (b) positive measurement bias on the FM electrode. The dashed line is the Fermi level in STO, the grey area represents the filled states of Co. (c) Illustration of our model inspired from Ref. [14] whereby electrons transit *via* discrete states in which the spin is depolarized by a field H_r . Physical parameters are defined in the text.

To get insight into these possible random fields, we measured the inverted Hanle effect (dark blue points, H_{\parallel} configuration), that is compared to the normal Hanle effect (light blue points, H_{\perp} configuration) in Fig. 2(d). Both Hanle and inverted Hanle data can be fitted by a Lorentzian plus the same parabolic background. Quantitatively, the inverted Hanle signal is equal to $\Delta R_{H\parallel}A \approx 0.24 \text{ G}\Omega \cdot \mu\text{m}^2$, and thus the total Hanle signal $\Delta R_{HA} = \Delta R_{H\perp}A + \Delta R_{H\parallel}A \approx 0.3 \text{ G}\Omega \cdot \mu\text{m}^2$, corresponding to a $MR = 0.4\%$. Striking similarities with the signals obtained for FM/AIO₂/Si junctions [13] indicate a gradual restoration of the spin accumulation to its maximum value for an in-plane field of about 0.2 T. Then, the total amplitude of the spin accumulation scales with ΔR_{HA} . According to this picture and in the limit of a long spin-lifetime, the voltage variation equals $\Delta V = |\frac{2}{\Delta} \Delta\mu/e| \langle \cos^2(\theta) \rangle$, where θ is the average angle between the spin direction and the local magnetic field that is the sum of a random field H_r fluctuating in space and the external field H_{ext} . Consequently the amplitude of the inverted Hanle signal should be 2/3 of the total signal if H_r were perfectly random. As in the case of hybrid organic spin valves [34] or ZnO oxide quantum dots [35], we believe that H_r may originate from the hyperfine interactions [36,37] with Al³⁺ and La³⁺ nuclei bearing a nuclear moment of $I_{\text{Al}} = 5/2$ for ²⁷Al (with a 100% abundance) and $I_{\text{La}} = 7/2$ for ¹³⁹La (with a 99.91% abundance) [38] and associated to residual oxygen vacancies or intermixing species in LAO. In this scenario, electrons are likely subject to a random field $H_r = \frac{2}{3} \mu_0 g_n \mu_B \hbar \vec{I} \cdot \vec{S} |\psi(0)|^2$ where g_n is the nuclear gyromagnetic ratio ($g_n^{\text{Al}} = 1.4566$, $g_n^{\text{La}} = 0.7952$) and $\psi(0)$ is the weight of their respective 3s- and 6s-type wave function at the

nuclei. H_r is estimated to be about 0.1–0.2 T for Al and La taking into account the typical extension of their wave function [39] in good agreement with the width of the inverted Hanle MR curve.

Applying a gate voltage V_g at the back of the STO substrate [see Fig. 1(a)] can give further information about the phenomena at play. Besides modulating the carrier concentration at the LAO/STO interface [5–7], V_g may also strongly modify their confinement in the direction perpendicular to the interface, as calculated in Ref. [7]. Figure 4 displays the effect of V_g across the 0.5 mm thick STO substrate where a positive gate-voltage results in an accumulation of electrons in the 2-DES accompanied by a reduction of the sheet resistance R_{\square} of the 2-DES (green line on Fig. 4(d)), typically by 1 order of magnitude [5–9]. Quite surprisingly, V_g has an opposite effect upon ΔR_{HA} with respect to R_{\square} [Fig. 4(b) and 4(d)]. This goes against what one expects for the variation of the *intrinsic* 2-DES spin resistance (R_{ch}^s) vs V_g that should follow the variation of R_{\square} in the linear regime of spin injection [40].

Moreover, the total Hanle signal ΔR_{HA} is enhanced by 5 to 6 orders of magnitude compared to its expected value $R_{\text{ch}}^s = R_{\square} \cdot \ell_{\text{sf}}^2$, derived from the standard theory of spin injection [25] and evaluated at $\approx 200 \Omega \cdot \mu\text{m}^2$ for $R_{\square} = 0.2 \text{ k}\Omega$ and a spin-diffusion length of the order $\ell_{\text{sf}} = \sqrt{D\tau_{\text{sf}}} \approx 1 \mu\text{m}$ ($\tau_{\text{sf}} \approx 1 \text{ ps}$), where D is the diffusion constant in the channel. A probable scenario to explain both the amplification of the spin signal and its singular gate-voltage dependence is that of Ref. [14] that invokes a

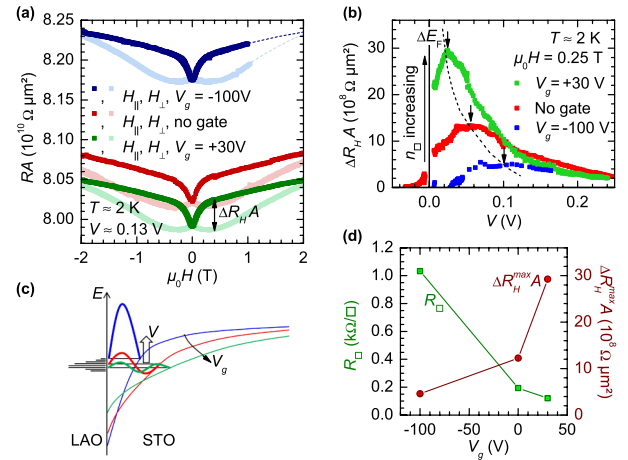


FIG. 4 (color online). (a) MR of the Co/LAO/STO structure in H_{\perp} and H_{\parallel} configurations for different gate voltage V_g at 2 K. (b) Total Hanle signal ΔR_{HA} (evaluated at 0.25 T) vs measurement bias V applied across the Co/LAO/STO junction at different V_g . Arrows indicate $\Delta R_{HA}^{\text{max}}A$ (c) Sketch of the 2-DES band structure evolution vs V_g , illustrating the loss of carrier confinement in the 2-DES (decrease of k_{\perp}) as V_g increases. (d) V_g dependence of the various resistances, showing the singular increase of the total spin signal $\Delta R_{HA}^{\text{max}}A$ vs V_g , whereas the sheet resistance of the channel R_{\square} decreases as expected [5–9].

spin injection process into resonant electronic localized states (ELS). We apply it to spin injection into our LAO/STO interfaces in the following.

The prerequisites for spin amplification are that these ELS form a narrow band of reduced density-of-states (DOS) and enhanced spin-lifetime $\tau_{\text{sf}}^{\text{ELS}}$ due to localization effects [see Fig. 3(c)]. This leads to a spin accumulation $\Delta\mu_{\text{ELS}}$ in the ELS of the form given in Ref. [14]. Neglecting the channel resistance compared to the tunnel resistances, we have here

$$\Delta\mu_{\text{ELS}} \simeq e\gamma J \frac{R_{\text{ELS}}^s \cdot r_b}{R_{\text{ELS}}^s + r_b} \quad (1)$$

or, equivalently,

$$\Delta\mu_{\text{ELS}} \simeq \frac{\gamma J}{e\mathcal{N}_{2-D}^{\text{ELS}}} \frac{\tau_{\text{sf}}^{\text{ELS}} \cdot \tau_{\rightarrow}^{\text{ELS}}}{\tau_{\text{sf}}^{\text{ELS}} + \tau_{\rightarrow}^{\text{ELS}}}, \quad (2)$$

where J is the injected current density, $R_{\text{ELS}}^s = \tau_{\text{sf}}^{\text{ELS}}/(e^2\mathcal{N}_{2-D}^{\text{ELS}})$ the spin-flip resistance of the ELS, and $r_b = \tau_{\rightarrow}^{\text{ELS}}/(e^2\mathcal{N}_{2-D}^{\text{ELS}})$ the coupling tunnel resistance between the ELS and the 2-DES. Here, $\mathcal{N}_{2-D}^{\text{ELS}}$ is the two-dimensional ELS-DOS and $\tau_{\rightarrow}^{\text{ELS}}$ is the characteristic tunneling escape time from the ELS towards the 2-DES.

While V_g is not expected to influence the spin lifetime on the localized states $\tau_{\text{sf}}^{\text{ELS}}$, it may strongly affect the escape time of the electrons from the localized states to the 2-DES $\tau_{\rightarrow}^{\text{ELS}}$ by changing the tunneling coupling between the two. This coupling is parameterized by the characteristic elastic energy broadening $\Gamma_R \approx \frac{\hbar}{\tau_{\rightarrow}^{\text{ELS}}}$ according to [41]:

$$\Gamma_R \approx \frac{2k^\perp\chi}{(k^\perp)^2 + \chi^2} [\epsilon_i] \frac{\exp(-2\chi \cdot d)}{\chi \cdot d}, \quad (3)$$

where ϵ_i is the localization energy, $1/\chi$ the characteristic localization length of the ELS, k^\perp the carrier wave-vector in the 2-DES along the growth direction (confinement axis), and d the tunneling distance. In the highly localized limit ($\chi \gg k^\perp$), $\Gamma_R \propto \frac{2k^\perp}{d} \exp(-2\chi \cdot d)$, and $\tau_{\rightarrow}^{\text{ELS}} \propto 1/k^\perp$. A smaller carrier confinement in the 2-DES by a positive V_g (that enhances the 2-DES DOS and thus the sheet conductance $1/R_\square$ but reduces k^\perp) then leads to an increase of the escape time $\tau_{\rightarrow}^{\text{ELS}}$, resulting in scaling up r_b . From Eq. (1), $\Delta\mu_{\text{ELS}}$ thus increases and so does ΔR_{HA} . On the contrary, a larger confinement in the 2-DES by a negative V_g (that increases k^\perp) corresponds to a smaller escape time leading to a drop-off of ΔR_{HA} . This is just what we observe experimentally [see Fig. 4(b)]. Remarkably, the maximum ΔR_{HA} varies by 1 order of magnitude with V_g , which indicates that $r_b \ll R_{\text{ELS}}^s$, i.e., $\tau_{\rightarrow}^{\text{ELS}} \ll \tau_{\text{sf}}^{\text{ELS}}$. In other words, the spin lifetime is much longer than the escape time, which indicates spin conservation on the ELS and thus the creation of a finite spin accumulation in the channel due to the tunnel coupling. Finally, note that the maxima of the spin signal ΔR_{HA}

shifts with the gate voltage [dashed line in Fig. 4(b)], indicating a shift of the Fermi level in the 2-DES due to a change of the confinement potential of the well in STO at LAO/STO interface [see the sketch in Fig. 4(c)].

In conclusion, we have demonstrated the electrical spin injection from a magnetic tunnel contact to the LaAlO₃/SrTiO₃ interface system by measuring the Hanle effect with the magnetic field applied perpendicular or parallel to the sample plane. Our observation of strongly enhanced Hanle signals is consistent with a two-step tunneling process via localized electronic states of small DOS and enhanced spin lifetime in LaAlO₃, possibly played by oxygen vacancies and/or intermixing. The efficiency of spin injection into the 2-DES at the LAO/STO interface is discussed in terms of the coupling tunnel resistance with these localized electronic states controlled by the application of a backgate voltage. The observation of a significant gate-dependence of the spin signal as demonstrated here is due to a spin-lifetime on the localized states much longer than the escape time, possibly reaching values in the nanosecond range or beyond [42]. Importantly, this implies an efficient spin injection into the 2-DES itself with a maximized spin accumulation on the order of $\gamma R_{\text{ch}}^s J$ arising from spin-conserving tunneling transfer between the ELS and the 2-DES. Nevertheless, the spin signal in the 2-DES would not exceed 100 pV for a typical spin lifetime $\tau_{\text{sf}}^{\text{ch}} = 100$ ps and the current density ($100 \mu\text{A}/\text{cm}^2$) used for these tunnel junctions, which is hardly detectable by conventional measurement techniques.

To eventually detect the *direct* injection of spin-polarized carriers into the LAO/STO channel, either the injection contact resistance must be significantly reduced, replacing LAO by a lower bandgap material, or four-contact nonlocal detection schemes must be implemented. This will require distances between injector and detector smaller than the characteristic spin-diffusion length, which should be achievable with electron-beam lithography techniques. Resorting to lightly doped STO films with higher electron mobilities [43,44] may be another way to reduce the constraints on channel dimensions.

We would like to thank R. Bernard and E. Jacquet for help with the PLD system, and D. Sando for a careful reading of the manuscript. This work was supported by the French RTRA Triangle de la Physique and the French ANR Oxitronics (ANR-Blanc08-2-341281).

*henri.jaffres@thalesgroup.com

- [1] A. Ohtomo and H. Y. Hwang, *Nature (London)* **427**, 423 (2004).
- [2] P. Zubko, S. Gariglio, M. Gabay, P. Ghosez, and J.-M. Triscone, *Annu. Rev. Condens. Matter Phys.* **2**, 141 (2011).

- [3] M. Bibes, J.E. Villegas, and A. Barthélémy, *Adv. Phys.* **60**, 5 (2011).
- [4] N. Reyren *et al.*, *Science* **317**, 1196 (2007).
- [5] S. Thiel, G. Hammerl, A. Schmehl, C. W. Schneider, and J. Mannhart, *Science* **313**, 1942 (2006).
- [6] A.D. Caviglia, S. Gariglio, N. Reyren, D. Jaccard, T. Schneider, M. Gabay, S. Thiel, G. Hammerl, J. Mannhart, J.-M. Triscone, *Nature (London)* **456**, 624 (2008).
- [7] C. Bell, S. Harashima, Y. Kozuka, M. Kim, B. G. Kim, Y. Hikita, and H. Y. Hwang, *Phys. Rev. Lett.* **103**, 226802 (2009).
- [8] M. Ben Shalom, M. Sachs, D. Rakhmilevitch, A. Palevski, and Y. Dagan, *Phys. Rev. Lett.* **104**, 126802 (2010).
- [9] A.D. Caviglia, M. Gabay, S. Gariglio, N. Reyren, C. Cancellieri, J.-M. Triscone, *Phys. Rev. Lett.* **104**, 126803 (2010).
- [10] O. Copie *et al.*, *Phys. Rev. Lett.* **102**, 216804 (2009).
- [11] C. Cen, S. Thiel, J. Mannhart, J. Levy, *Science* **323**, 1026 (2009).
- [12] R. Jany *et al.*, *Appl. Phys. Lett.* **96**, 183504 (2010).
- [13] S. P. Dash, S. Sharma, J. C. Le Breton, J. Peiro, H. Jaffrès, J.-M. George, A. Lemaître, and R. Jansen, *Phys. Rev. B* **84**, 054410 (2011).
- [14] M. Tran, H. Jaffrès, C. Deranlot, J.-M. George, A. Fert, A. Miard, and A. Lemaître, *Phys. Rev. Lett.* **102**, 036601 (2009).
- [15] X. Lou, C. Adelman, M. Furis, S. A. Crooker, C. J. Palmström, and P. A. Crowell, *Phys. Rev. Lett.* **96**, 176603 (2006).
- [16] S. P. Dash, S. Sharma, R. S. Patel, M. P. de Jong, and R. Jansen, *Nature (London)* **462**, 491 (2009).
- [17] Y. Ando *et al.*, *Appl. Phys. Lett.* **99**, 132511 (2011).
- [18] T. Sasaki, T. Oikawa, T. Suzuki, M. Shiraishi, Y. Suzuki, and K. Noguchi, *Appl. Phys. Lett.* **96**, 122101 (2010).
- [19] T. Suzuki, T. Sasaki, T. Oikawa, M. Shiraishi, Y. Suzuki, and K. Noguchi, *Appl. Phys. Express* **4**, 023003 (2011).
- [20] C. H. Li, O. M. J. van't Erve, and B. T. Jonker, *Nature Commun.* **2**, 245 (2011).
- [21] A. Jain *et al.*, *Appl. Phys. Lett.* **99**, 162102 (2011).
- [22] C. W. Schneider, S. Thiel, G. Hammerl, C. Richter, and J. Mannhart, *Appl. Phys. Lett.* **89**, 122101 (2006).
- [23] C. Cancellieri, N. Reyren, S. Gariglio, A. D. Caviglia, A. Fête, and J.-M. Triscone, *Europhys. Lett.* **91**, 17004 (2010).
- [24] M. Basletic, J.-L. Maurice, C. Carrétéro, G. Herranz, O. Copie, M. Bibes, É. Jacquet, K. Bouzehouane, S. Fusil, and A. Barthélémy, *Nature Mater.* **7**, 621 (2008).
- [25] A. Fert and H. Jaffrès, *Phys. Rev. B* **64**, 184420 (2001).
- [26] G. Singh-Bhalla, C. Bell, J. Ravichandran, W. Siemons, Y. Hikita, S. Salahuddin, A. F. Hebard, H. Y. Hwang, and R. Ramesh, *Nature Phys.* **7**, 80 (2011).
- [27] K. Yoshimatsu, R. Yasuhara, H. Kumigashira, and M. Oshima, *Phys. Rev. Lett.* **101**, 026802 (2008).
- [28] X. Luo, B. Wang, and Y. Zheng, *Phys. Rev. B* **80**, 104115 (2009).
- [29] Z. Zhong, P. X. Xu, and P. Kelly, *Phys. Rev. B* **82**, 165127 (2010).
- [30] N. Nakagawa, H. Y. Hwang, and D. A. Muller, *Nature Mater.* **5**, 204 (2006).
- [31] S. A. Pauli, S. J. Leake, B. Delley, M. Björck, C. W. Schneider, C. M. Schlepütz, D. Martocchia, S. Paetel, J. Mannhart, and P. R. Willmott, *Phys. Rev. Lett.* **106**, 036101 (2011).
- [32] A. Fert, J.-M. George, H. Jaffrès, and R. Mattana, *IEEE Trans. Electron Devices* **54**, 921 (2007).
- [33] V. Garcia, M. Bibes, J.-L. Maurice, E. Jacquet, K. Bouzehouane, J.-P. Contour, and A. Barthélémy, *Appl. Phys. Lett.* **87**, 212501 (2005).
- [34] J. J. H. M. Schoonus, P. G. E. Lumens, W. Wagemans, J. T. Kohlhepp, P. A. Bobbert, H. J. M. Swagten, and B. Koopmans, *Phys. Rev. Lett.* **103**, 146601 (2009).
- [35] W. K. Liu, K. M. Whitaker, A. L. Smith, K. R. Kittilstved, B. H. Robinson, and D. R. Gamelin, *Phys. Rev. Lett.* **98**, 186804 (2007).
- [36] D. Paget, G. Lampel, B. Sapoval, and V. I. Safarov, *Phys. Rev. B* **15**, 5780 (1977).
- [37] I. A. Merkulov and A. L. Efros, *Phys. Rev. B* **65**, 205309 (2002).
- [38] See the nuclear isotope database at <http://www.easyspin.org/documentation/isotopetable.html>.
- [39] R. D. Cowan, *The Theory of Atomic Structure and Spectra* (University of California Press, Berkeley, Los Angeles, London, 1981), Chap. 7–8
- [40] Y. Ando *et al.*, *Appl. Phys. Lett.* **99**, 132511 (2011).
- [41] A. I. Larkin and K. A. Matveev, *Zh. Eksp. Teor. Fiz.* **93**, 1030 (1987) [*Sov. Phys. JETP* **66**, 580 (1988)].
- [42] S. Ghosh, V. Sih, W. H. Lau, D. D. Awschalom, S.-Y. Bae, S. Wang, S. Vaidya, and G. Chapline, *Appl. Phys. Lett.* **86**, 232507 (2005).
- [43] Y. Kozuka, M. Kim, C. Bell, B. G. Kim, Y. Hikita, and H. Y. Hwang, *Nature (London)* **462**, 487 (2009).
- [44] J. Son, P. Moetakef, B. Jalan, O. Bierwagen, N. J. Wright, R. Engel-Herbert, and S. Stemmer, *Nature Mater.* **9**, 482 (2010).